(Received 20 November 2023, Accepted 26 December 2023, Scheduled 12 January 2024)

An Enhanced Robustness Dual-Vector Model Predictive Torque Control for Permanent Magnet Synchronous Motors

Hao Xie[1], Cheng Zhang[1,2], Yang Zhang[1,*], and Sicheng Li[1]

[1] College of Electrical and Information Engineering, Hunan University of Technology, Zhuzhou 412007, China
[2] China Railway Signal and Communication (Changsha) Railway Traffic Control Technology Co. Ltd, Changsha 410000, China

ABSTRACT: The traditional dual-vector model predictive torque control (MPTC) of permanent magnet synchronous motor suffers from the problems of large control computation, large torque ripple, and prediction deviation due to parameter mismatch. To address these issues, an enhanced robustness dual-vector MPTC (ERD-MPTC) control strategy is proposed in this paper. First, in order to reduce the control computation, a fast voltage vector selection table based on a 12-sector voltage vector map is proposed, which reduces the number of prediction iterations from 14 to only 3. Secondly, to reduce the ripple of torque and flux in one cycle, the cost function without weight factor is proposed. This cost function includes fluctuations at the moment of the switching point. Then, for the bad effects of parameter mismatch, the inductance parameter is estimated by using the amount of error variation between the predicted value and the actual measured value at adjacent moments. So, an ERD-MPTC strategy to enhance the robustness of the prediction model in the presence of parameter mismatch is proposed by integrating the inductance updating mechanism and expanded state observer. Finally, through the experiment, it is shown that the proposed strategy can reduce the torque fluctuation, effectively reduce the adverse effects of parameter changes, and greatly improve the stability of the system.

1. INTRODUCTION

Permanent Magnet Synchronous Motor (PMSM) has the advantages of small size, simple structure, high control accuracy, etc., and is widely used in new energy vehicles, industrial robots, and other high-performance demand occasions [1, 2]. In recent years, in order to achieve high-performance control of permanent magnet synchronous motors, Finite-Control-Set Model Predictive Control (FCS-MPC) has become a hot spot of research with its advantages of fast dynamic response and easy nonlinear constraint processing [3–5]. According to the objectives of control, model predictive control is mainly divided into Model Predictive Torque Control (MPTC) [6] and Model Predictive Current Control (MPCC) [7]. The research on model predictive control algorithms has focused on steady state performance improvement, computational reduction, and parameter robustness enhancement.

Regarding the improvement of steady state performance and reduction of computation, [8] proposed Duty Cycle MPTC (DC-MPTC) to address the problem posed by the FCS-MPC with only a single vector in a cycle. By inserting a zero vector to regulate the action time of a voltage vector in a control cycle, the steady state performance of the system is improved. Reference [9] extends the second voltage vector to an arbitrary fundamental voltage vector, thus widening the choice of voltage vectors and reducing torque ripple to some extent. However, the optimization process has a large number of iterations, large computation volume, and high requirements for hardware equipment. Reference [10] proposed an improved dual-vector MPTC based on optimized duty cycle, with the proposed voltage vector selection table reducing the number of iterations, but the subsequent optimization of the vector action time is more complicated. Later, three-vector MPTC was proposed to act as three voltage vectors in one control cycle, with the last one being the zero vector, and [11–13] show the three-vector MPTC strategy. The three-vector MPTC requires an optimization search for the combination of voltage vectors in each sector within one control cycle, and also an optimization calculation of the action time of the three voltage vectors, resulting in a still larger computational amount of this control strategy and increases the inverter switching frequency.

The cost function is also one of the determinants of the control performance [14], and the cost function of the traditional MPTC has weight factors difficult to be rectified, thus increasing the complexity of the algorithm [15, 16]. In addition to this, the above strategy only focuses on the tracking effect at the end of the cycle and ignores the volatility at the moment of the switching point. Reference [17] proposed new hysteresis controllers and divided the voltage vector map into 12 sectors, so as to effectively reduce the computation. Reference [18] quickly selects a valid voltage vector and predicts it only once by sectorization, and the selected combination of voltage vectors may not be the optimal combination due to too many excluded voltage vectors.

In terms of parameter robustness improvement, [19] introduced an online parameter identification link to continuously update the prediction model online, improving the control accuracy in case of parameter mismatch. The observer is a good solution in dealing with parameter mismatch as well as disturbance problems, with more flexible applications and design approaches than parameter identification. In [20], parameter

* Corresponding author: Yang Zhang (459387623@qq.com).

mismatch disturbance, external disturbance, and uncertainty are used as the total disturbance to design expanded state observer (ESO), effectively solving the system noise problem caused by parameter mismatch disturbance. Reference [21] used an incremental form of the model and a disturbance observer that eliminates the flux parameter and improves the parameter robustness. Reference [22] is based on the method of disturbance observation to compensate the parameter errors and internal and external disturbances by observation. However, the algorithm designs in [20–22] are all overly complex, placing an increased burden on the controller and potentially requiring additional error compensation. In addition, the measured values can be used to replace the motor parameters in the model predictive control, which is very helpful to improve the robustness of the drive control strategy to parameter mismatch. Therefore, many scholars have also devoted themselves to reducing the use of motor parameters in the drive control process [23–25]. References [26, 27] realized the method of replacing motor parameters by measured values and showed better control results.

To address the problems, this paper proposes an enhanced robustness dual-vector MPTC (ERD-MPTC) strategy. Three candidate dual-vector combinations are quickly selected based on a fast voltage vector selection table; subsequently, a cost function in the form of relative error rates of torque and flux is used to eliminate the weight factor. The fluctuation of the switching point moment is considered in the cost function, and an improved dual-vector MPTC (ID-MPTC) is also proposed. Compared to the traditional dual-vector MPTC, which requires 14 predictions, the improved strategy requires only 3 predictions. It not only reduces the complexity of the control algorithm, but also ensures that the selected vector combination has small torque and flux ripple throughout the cycle. In addition, in order to avoid the parameter mismatch from bringing poor control performance to the motor, a control method to enhance the robustness by integrating the inductance updating mechanism and the expanded state disturbance observer is proposed to improve the robustness of the predictive model parameters during parameter mismatch based on the ID-MPTC. Finally, the control strategy proposed is experimentally proved to be effective.

2. MATHEMATICAL MODEL OF PMSM

In this paper, surface PMSM (SPMSM) is the object of research. The core saturation in the motor is neglected, and the eddy current and hysteresis losses in the motor are not taken into account. The stator voltage equation and flux equation of the PMSM in the synchronous rotating coordinate system (*dq*) are expressed as follows [28]:

$$\begin{cases} u_d = Ri_d + \frac{d\psi_d}{dt} - \omega_e L_q i_q \\ u_q = Ri_q + \frac{d\psi_q}{dt} + \omega_e L_d i_d + \omega_e \psi_f \end{cases} \tag{1}$$

$$\begin{cases} \psi_d = L_d i_d + \psi_f \\ \psi_q = L_q i_q \end{cases} \tag{2}$$

In the *dq* coordinate system, the mathematical model of PMSM achieves decoupling, and the electromagnetic torque equation can be expressed as:

$$T_e = \frac{3p}{2L_s}\,\psi_s \otimes \psi_f = \frac{3}{2}\,p_n i_q \left[i_d\left(L_d - L_q\right) + \psi_f\right] \tag{3}$$

where u_d, u_q are the *dq*-axis components of the stator voltage; i_d, i_q are the *dq*-axis components of the stator current; ψ_d, ψ_q are the *dq*-axis components of the stator flux; ψ_f is the permanent magnet flux; ω_e is the rotor electrical angular velocity; R_s is the stator resistance; P_n is the number of pole pairs of the PMSM; and the *dq*-axis inductances of the SPMSM are equal, i.e., $L_s = L_d = L_q$. Then Equation (3) can be rewritten as:

$$T_e = \frac{3}{2}\,p_n \psi_f i_q \tag{4}$$

In order to obtain the predicted values of torque and stator flux, a first-order expansion of Eq. (1) in terms of Taylor series can transform the continuous model into a discrete prediction model, then

$$\begin{cases} i_d^{k+1} = \left(1 - \frac{R_s}{L_s}\,T_s\right) i_d^k + T_s \omega_e i_q^k + \frac{T_s}{L_s}\,u_d^k \\ i_q^{k+1} = \left(1 - \frac{R_s}{L_s}\,T_s\right) i_q^k + T_s \omega_e i_d^k - \frac{T_s}{L_s}\,\psi_f \omega_e + \frac{T_s}{L_s}\,u_q^k \end{cases} \tag{5}$$

$$\begin{bmatrix} \psi_d^{k+1} \\ \psi_q^{k+1} \end{bmatrix} = \begin{bmatrix} L_d & 0 \\ 0 & L_q \end{bmatrix} \begin{bmatrix} i_d^{k+1} \\ i_q^{k+1} \end{bmatrix} + \begin{bmatrix} \psi_f \\ 0 \end{bmatrix} \tag{6}$$

$$\psi_s^{k+1} = \sqrt{\left(\psi_d^{k+1}\right)^2 + \left(\psi_q^{k+1}\right)^2} \tag{7}$$

$$T_e^{k+1} = \frac{3}{2}\,p_n \psi_f i_q^{k+1} \tag{8}$$

in Eqs. (5)∼(8), x^k means the value of the physical variable x at the current k moments; x^{k+1} means the predicted value of the physical variable x at the $k+1$ moments; and T_s is the discrete period.

A three-phase two-level voltage-type converter can generate eight fundamental voltage vectors, where six are active vectors, and the other two are zero vectors, by control of the on and off switching of the upper and lower bridge arm switching tubes.

$$\mathbf{u}_j = \frac{2}{3}\,V_{dc}\left(S_a + S_b\,e^{j\frac{2\pi}{3}} + S_c\,e^{j\frac{4\pi}{3}}\right) \tag{9}$$

where $\mathbf{u}_j$ $(j = 0 \sim 7)$ denotes the fundamental voltage vector; $\mathbf{u}_0$ and $\mathbf{u}_7$ are two zero vectors; V_{dc} is the bus voltage on the DC side; S_a, S_b, S_c are the switching states of the upper and lower bridge arms of the three-phase inverter.

3. TRADITIONAL DUAL-VECTOR MPTC

The traditional dual-vector MPTC is an improvement on the duty cycle control strategy. From the original second voltage vector can only be zero vector; it is extended to the candidate vectors for the second voltage vector are seven voltage vectors.

The basic control strategy of the traditional dual-vector MPTC is as follows: Step 1, conduct the first round of selection using the cost function to screen out the first optimal vector

$\mathbf{u}_{\text{opt1}}$. Step 2, preassign the action time between $\mathbf{u}_{\text{opt1}}$ and the seven basic voltage vectors in one cycle based on deadbeat torque control principle. Then seven dual-vector combinations can be obtained. Step 3, substitute the predicted values of the seven dual-vector combinations into the cost function for the second round of selection, so that the dual-vector combination with the smallest value of the cost function is the optimal combination.

The traditional dual-vector MPTC performs two rounds of screening prediction in one control cycle with a total of 14 prediction iterations. In step 1 above, each of the seven voltage vectors needs to be substituted into the prediction equations (5)∼(7) to obtain seven sets of torque and flux chain prediction values, which are then substituted into the cost function equation (16) for screening. A total of 7 predictions are required to complete this round of predictive control. The dual-vector MPTC needs to act on two voltage vectors in one control cycle, then it is necessary to allocate the time for the two voltage vectors to act in one cycle. Step 2 is the allocation of the action time when $\mathbf{u}_{\text{opt1}}$ is combined with each of the seven voltage vectors under torque deadbeat control. Step 3 is using the seven dual-vector combinations obtained in Step 2 for prediction and then substituting them into the cost function selection, similar to Step 1. To complete this round of predictive control, it is also necessary to make 7 predictions. The algorithm requires a total of 14 predictions for the two rounds of screening, resulting in a large control computation.

3.1. Traditional Dual-Vector Combination Selection and Action Time Allocation

Assume that the elected first voltage vector is $\mathbf{u}_{\text{opt1}}$, and the action time is t_{opt1}. Using the deadbeat torque control principle to distribute the action time, so that the torque value at the end of the next moment is equal to the given value, i.e., $T_e^* = T_e^{k+1}$. Then

$$T_e^{k+1} = T_e^* = T_e^k + S_{\text{opt1}} t_{\text{opt1}} + S_j \left(T_s - t_{\text{opt1}}\right) \tag{10}$$

where S_{opt1} and S_j $(j = 0 \sim 7)$ are the torque slopes of the first and second voltage vectors, respectively.

$$\begin{aligned} S_{\text{opt1}} &= \left.\frac{dT_e}{dt}\right|_{u_s = u_{\text{opt1}}} \\ &= \frac{1}{L_s}\left[-R_s T_e^k - \frac{3}{2} p_n \omega_e^k \psi_f \psi_d^k + \frac{3}{2} p_n \psi_f u_{q\_\text{opt1}}^k\right] \end{aligned} \tag{11}$$

$$\begin{aligned} S_j &= \left.\frac{dT_e}{dt}\right|_{u_s = u_j} \\ &= \frac{1}{L_s}\left[-R_s T_e^k - \frac{3}{2} p_n \omega_e^k \psi_f \psi_d^k + \frac{3}{2} p_n \psi_f u_{q\_j}^k\right] \end{aligned} \tag{12}$$

in Eqs. (11) and (12), u_{q_opt1} and u_{q_j} $(j = 0 \sim 7)$ denote the q-axis components of the first and second voltage vectors; the dq-axis component of the zero vector is 0.

According to Eq. (13), the action time t_{opt1} of the first voltage vector can be obtained, and then the action time of the second voltage vector is T_s-t_{opt1}.

$$t_{\text{opt1}} = \frac{T_e^* - T_e^k - T_s S_j}{S_{\text{opt1}} - S_j} \tag{13}$$

$$t_{\text{opt1}} = \begin{cases} T_s & (t_{\text{opt1}} > T_s) \\ 0 & (t_{\text{opt1}} < 0) \end{cases} \tag{14}$$

The stator currents i_d, i_q of the seven candidate voltage vector combinations can be predicted by using the voltage model Eq. (15), respectively. Then substitute the obtained i_d^{k+1}, i_q^{k+1} into Eqs. (6), (7), and (8) to obtain the seven sets of ψ_s^{k+1} and T_e^{k+1}, for the subsequent screening of the cost function.

$$\begin{cases} u_{sd} = \frac{t_{\text{opt1}}}{T_s} u_{d\_\text{opt1}} + \frac{T_s - t_{\text{opt1}}}{T_s} u_{d\_j} \\ u_{sq} = \frac{t_{\text{opt1}}}{T_s} u_{q\_\text{opt1}} + \frac{T_s - t_{\text{opt1}}}{T_s} u_{q\_j} \end{cases} \tag{15}$$

where u_{d_opt1} and u_{q_opt1} are the dq-axis components of the first voltage vector in the two-vector combination; u_{d_j} and u_{q_j} are the dq-axis components of the second voltage vector in the dual-vector combination; u_{sd} and u_{sq} are the dq-axis components of the stator current; and the dq-axis component of the zero vector is 0.

3.2. Traditional Strategy Cost Function

Due to the different magnitudes of torque and flux, it is necessary to set the weight factor to balance the relationship between the torque and flux errors in the cost function. The traditional cost function is in the form of error tracking, as in Eq. (16)

$$g = \left|T_e^* - T_e^{k+1}\right| + Q\left|\psi_s^* - \psi_s^{k+1}\right| \tag{16}$$

where T_e^* and ψ_s^* are the reference values of torque and stator flux respectively; Q is the weighting factor, and the traditional algorithms generally use empirical collocation or set the torque and flux to have equally important weights.

4. ENHANCED ROBUSTNESS DUAL-VECTOR MPTC STRATEGY (ERD-MPTC)

4.1. The Proposed Improved Dual-Vector MPTC (ID-MPTC)

This paper proposes an improved dual-vector MPTC (ID-MPTC) control strategy. Firstly, the vector sector distribution map is reclassified, and a fast selection table is obtained according to the control demand. Compared with the traditional dual-vector MPTC, the proposed fast voltage vector selection table omits step 1 in the traditional dual-vector MPTC control algorithm and also optimizes the number of predictions in step 3. The traditional dual-vector MPTC requires 14 predictions, while the vector selection table proposed in this paper requires only 3 predictions for voltage vector selection, which reduces the computation amount. Secondly, a cost function in the form of relative error rates of torque and flux is used to eliminate the weight factor, which avoids the complicated rectification of the weight factor. And the torque and flux of the switching point moments are taken into account in the cost function.

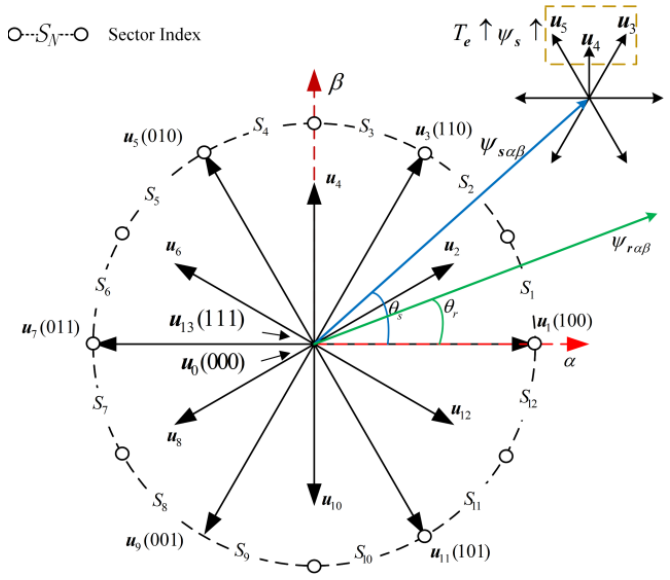

FIGURE 1. Voltage vector sector distribution map and examples of the effect on torque and stator flux.

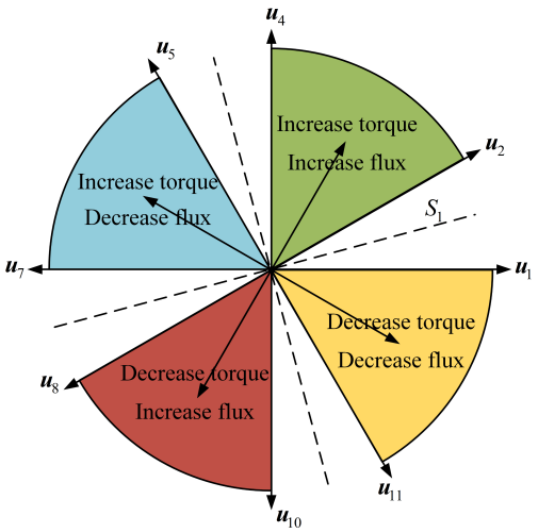

FIGURE 2. Classification of voltage vectors in the S_1 sector.

4.1.1. Dual-Vector Combination Principle

In order to improve the control accuracy and reduce the current harmonics, the voltage vector sector map is redivided into 12 sectors in this paper, and the angle occupied by each sector is 30°, as shown in Fig. 1. The sector division satisfies Eq. (17), and S_N $(N = 1, 2, ..., 12)$ is the sector index. The two zero vectors $\mathbf{u}_0(000)$ and $\mathbf{u}_{13}(111)$ have the same effect on torque control, and this paper will uniformly refer to the zero vector $\mathbf{u}_0$.

$$(2N-2)\frac{\pi}{12} \le S_N \le 2N\frac{\pi}{12} \tag{17}$$

Based on the six active vectors, the neighbouring voltage vectors are combined two by two, constituting six sets of dual voltage vector combinations, generating six virtual vectors, including $\mathbf{u}_2(\mathbf{u}_1, \mathbf{u}_3)$, $\mathbf{u}_4(\mathbf{u}_3, \mathbf{u}_5)$, $\mathbf{u}_6(\mathbf{u}_5, \mathbf{u}_7)$, $\mathbf{u}_8(\mathbf{u}_7, \mathbf{u}_9)$, $\mathbf{u}_{10}(\mathbf{u}_9, \mathbf{u}_{11})$, and $\mathbf{u}_{12}(\mathbf{u}_{11}, \mathbf{u}_1)$ as shown in Fig. 1. The combinatorial relationship between each virtual vector and the active vector satisfies

$$\mathbf{u}_i = \frac{t_{i,u_m}}{T_s}\mathbf{u}_m + \frac{t_{i,u_n}}{T_s}\mathbf{u}_n \tag{18}$$

in Eq. (18), u_i $(i = 2, 4, ..., 12)$ is the synthesized virtual vector; u_m $(m = 1, 3, ..., 11)$, u_n $(n = 1, 3, ..., 11)$ are the neighbouring two active voltage vectors of the inverter; t_{i,u_m}, t_{i,u_n} are the action time of u_m and u_n, respectively, and satisfies

$$t_{i,u_m} + t_{i,u_n} = T_s \tag{19}$$

The voltage selection for the method proposed in this paper involves torque error and stator flux error, here defined as torque error ΔT_e and stator flux error $\Delta\psi_s$.

$$\begin{cases} \Delta T_e = T_e^* - T_e \\ \Delta\psi_s = \psi_s^* - \psi_s \end{cases} \tag{20}$$

If $\Delta T_e \ge 0$, it means that the torque needs to be increased, and if $\Delta\psi_s \ge 0$, it means that the stator flux amplitude needs to be increased. Similarly, $\Delta T_e < 0$ needs to decrease the torque, and $\Delta\psi_s < 0$ needs to decrease the stator flux amplitude.

Based on the concept of load angle and Equation (4), the electromagnetic torque can again be expressed as:

$$T_e = \frac{3}{2}\frac{p_n\,|\psi_s|}{L_d}\,(\psi_f \sin\delta) \tag{21}$$

where δ is the load angle.

Electrical parameters change much faster than mechanical parameters, and changes in the rotor flux are negligible over very short time intervals. That is, in the $\alpha\beta$ coordinate system, the stator flux position angle θ_s can be changed under the action of the voltage vector, but the rotor flux chain position θ_r is almost unchanged, thus changing the load angle $\delta = \theta_s - \theta_r$, which ultimately facilitates the control of the electromagnetic torque. Neglecting the stator resistance voltage drop, the proportional relationship between the voltage vector $\mathbf{u}_s$ and the flux vector ψ_s can be expressed as:

$$\Delta\vec{\psi}_s = \vec{\mu}_s \Delta t \tag{22}$$

Based on the switching table principle of direct torque control, it can be seen that the 12 voltage vectors (6 active vectors and 6 virtual vectors) can be classified into four categories according to the range of angles between the voltage vectors and the stator flux vectors: the clamping angle between 0° and 90° can increase torque and increase flux, between 90° and 180° can increase torque and decrease flux, between 180° and 270° can decrease torque and increase flux, and between 270° and 360° can decrease torque and decrease flux. In addition to the 6 active vectors, 6 virtual vectors are introduced. With this approach, for each category, there are 3 active or virtual vectors to satisfy the torque and flux control requirements. Take sector S_1 as an example, as shown in Fig. 2.

Candidate dual-vector combinations are determined according to the following principles: according to the sector where the stator flux is located, and then combined with the torque and chain error sign; when the active voltage vector meets the control requirements, the active vector is allowed to be used as the first voltage vector, and the zero vector is used as the second voltage vector; when the synthesized virtual voltage vector meets the control requirements, the dual-vector combination is selected as the virtual vector itself. The fast voltage vector selection Table for the proposed ID-MPTC method is shown in Table 1.

TABLE 1. Fast voltage vector selection table.

sector location	T_e	ψ_s	Candidate active voltage vectors or virtual vectors
S_N	↑	↑	$\mathbf{u}_{N+1}$, $\mathbf{u}_{N+2}$, $\mathbf{u}_{N+3}$
	↑	↓	$\mathbf{u}_{N+4}$, $\mathbf{u}_{N+5}$, $\mathbf{u}_{N+6}$
	↓	↑	$\mathbf{u}_{N-1}$, $\mathbf{u}_{N-2}$, $\mathbf{u}_{N-3}$
	↓	↓	$\mathbf{u}_{N-4}$, $\mathbf{u}_{N-5}$, $\mathbf{u}_{N-6}$

In Table 1, ↑ denotes the increasing torque or stator flux; ↓ denotes the decreasing torque or stator flux; and N ($N = 1, 2, 3, ..., 12$) is the sector index number. $N + k$ in the voltage vector is the voltage vector (u_{N+k}) selection index. When the parameter $N + k > 12$, the actual value of parameter $N + k$ is the value obtained by taking the remainder of $N + k$ to 12. When the parameter $N + k \leq 0$, the actual value of parameter $N + k$ is $N + k + 12$.

Figure 1 shows voltage vector sector distribution map and examples of the effect on torque and stator flux. Assume that the sector where the stator flux is situated is S_2 and that an increase of torque and an increase of flux are required. According to Fig. 1 and the fast voltage vector selection table, the 3 candidate voltage vectors combinations are ($\mathbf{u}_3$, $\mathbf{u}_0$), $\mathbf{u}_4$($\mathbf{u}_3$, $\mathbf{u}_5$), and ($\mathbf{u}_5$, $\mathbf{u}_0$). Zero vector can be directly involved in PMSM direct torque control to reduce torque ripple and will be selected based on the principle of minimum number of switching transitions. The same applies when the stator flux is rotated to other sectors. Since all the three candidate voltage vector combinations satisfy the system's demand for torque, to obtain a smaller torque ripple, the optimal set of inputs to the converter needs to be selected by the cost function.

4.1.2. Action Time Optimization and Cost Function Design

The proposed ID-MPTC strategy still assigns the action time of two voltage vectors using the deadbeat torque control principle, which can be used in Eq. (13) and Eq. (14) to obtain the first voltage vector action time t_{opt1}, then the second voltage vector action time is T_s-t_{opt1}. Based on the three candidate vectors obtained from Table 1, using Eq. (15) and Eqs. (6)∼(8), three sets of ψ_s^{k+1} and T_e^{k+1} can be obtained for subsequent cost function screening.

Equation (23) is the traditional error rate form of the cost function, and the cost function omits the setting and adjustment of the weight factor. This is because the relative error rate is used to realize the control of the flux and torque, which are dimensionless physical quantities of the same order of magnitude.

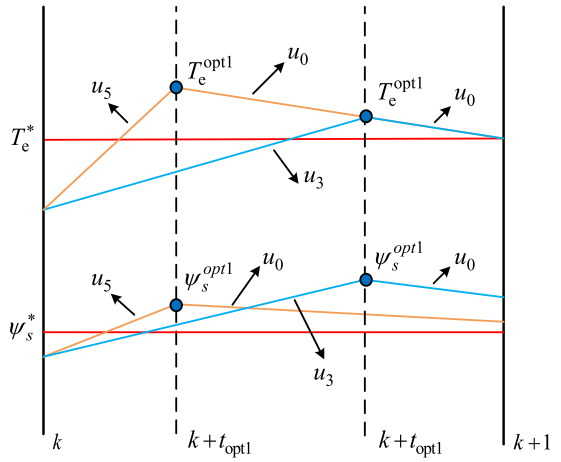

FIGURE 3. Two dual-voltage vector combinations schematically diagrammed.

At the end of the action of the first voltage vector, it switches to the second vector, which means that the t_{opt1} moment is the moment of the switching point in one cycle. Fig. 3 shows two dual-voltage vector combinations schematically diagrammed. As shown in the schematic of Fig. 3, the relative errors of the torque and the flux at the switching point can well reflect the fluctuation of the whole cycle. In this paper, the fluctuations at the moment of switching point are considered in the proposed cost function, as shown in Eq. (25). Since the torque has been deadbeat control, Eq. (24) can be simplified to Eq. (25). When making comparisons of function values, just calculate the squared term g^2. The proposed cost function takes the torque control performance into account along with some stator flux fluctuations.

$$g = \sqrt{\left[\frac{T_e^* - T_e^{k+1}}{T_e^*}\right]^2 + \left[\frac{\psi_s^* - \psi_s^{k+1}}{\psi_s^*}\right]^2} \tag{23}$$

$$g = \sqrt{\left[\frac{T_e^* - T_e^{\text{opt1}}}{T_e^{k*}}\right]^2 + \left[\frac{T_e^* - T_e^{k+1}}{T_e^*}\right]^2 + \left[\frac{\psi_s^* - \psi_s^{\text{opt1}}}{\psi_s^*}\right]^2 + \left[\frac{\psi_s^* - \psi_s^{k+1}}{\psi_s^*}\right]^2} \tag{24}$$

$$g = \sqrt{\left[\frac{T_e^* - T_e^{\text{opt1}}}{T_e^*}\right]^2 + \left[\frac{\psi_s^* - \psi_s^{\text{opt1}}}{\psi_s^*}\right]^2 + \left[\frac{\psi_s^* - \psi_s^{k+1}}{\psi_s^*}\right]^2} \tag{25}$$

in Eqs. (24)∼(25), T_e^{opt1}, ψ_s^{opt1} are the values of torque and flux at the moment of switching point, respectively.

4.1.3. Parameter Mismatch Analysis

From the prediction model, it can be seen that the model contains motor parameters such as stator resistance R_s, stator inductance L_s, and permanent magnet flux ψ_f, which are subject

to change by factors such as temperature rise and magnetic saturation, thus affecting the torque prediction. The stator resistance and permanent magnet flux are less sensitive to the prediction error than the stator inductance parameter, which is the most sensitive and has a greater impact on the control performance of the system.

The torque prediction error for parameter mismatch is

$$\Delta T_{ep} = \tilde{T}_e^{k+1} - T_{ep}^{k+1} \tag{26}$$

If only the inductor parameter mismatch is considered, the torque prediction error can be expressed as:

$$\Delta T_L^p = \left| \frac{1.5 p_n \psi_f \Delta L T_s}{L_s \left(L_s + \Delta L\right)} \left(-u_q^k + R_s i_q^k\right) \right| \tag{27}$$

in Eqs. (26) and (27), T_{ep}^{k+1} is the torque prediction value at time $k+1$ when the parameter is accurate; $\tilde{T}_e^{k+1}$ is the predicted value of torque at $k+1$ moment of parameter mismatch, and ΔT_L^p is the torque prediction error when the inductor parameter is mismatched; ΔL is the uncertainty component caused by the inductor parameter mismatch.

From Eq. (27), it is obvious that when the inductor parameters mismatch, it will cause a large torque prediction error, which further deteriorates the control system and causes a large torque ripple. Similar conclusions can be obtained for other parameter mismatches.

4.2. Enhanced Robustness Control Method

To reduce the harmful effects of parameter mismatch, the improved robustness control strategy extracts the inductance values using the predicted and actual sampled values of three adjacent cycles at k, $k-1$, and $k-2$, as well as the action time of the dual-vectors, thus updating the inductance to obtain a more accurate predicted value. Then, the ESO observer is used to capture other parameter variations as well as externally generated disturbances, which are compensated into the prediction model to achieve enhanced robustness of the ID-MTPC.

Set $\tilde{L}_s = L_s + \Delta L$, $\tilde{\psi}_f = \psi_f + \Delta\psi_f$, $\tilde{R}_s = R_s + \Delta R$; L_s, ψ_f, and R_s are the values of motor parameters in the prediction model in the absence of parameter mismatch; $\tilde{L}_s$, $\tilde{\psi}_f$, and $\tilde{R}_s$ are the actual values in the prediction model when parameter mismatch occurs; ΔL, $\Delta\psi_f$, and ΔR are the uncertainty components due to parameter mismatch of inductance, flux, and resistance, respectively.

4.2.1. Inductor Update Mechanism

When the parameters are accurate, the predicted current at moment k after discretization is obtained from Equation (5):

$$\begin{cases} i_{dp}^k = \left(1 - \frac{T_s R_s}{L_s}\right) i_d^{k-1} + T_s \omega_e i_q^{k-1} + \frac{1}{L_s} T_s u_{sd}^{k-1} \\ i_{qp}^k = \left(1 - \frac{T_s R_s}{L_s}\right) i_q^{k-1} - T_s \omega_e i_d^{k-1} \\ \qquad + \frac{1}{L_s} T_s u_{sq}^{k-1} - \frac{T_s \omega_e \psi_f}{L_s} \end{cases} \tag{28}$$

$$\begin{cases} T_s u_{sd}^{k-1} = t_1^{k-1} u_{1d}^{k-1} + t_2^{k-1} u_{2d}^{k-1} \\ T_s u_{sq}^{k-1} = t_1^{k-1} u_{1q}^{k-1} + t_2^{k-1} u_{2q}^{k-1} \end{cases} \tag{29}$$

in the above equation, i_{dp}^k and i_{qp}^k are the *dq*-axis predicted current at moment k; i_q^{k-1} and i_d^{k-1} are the *dq*-axis sampling current at the moment $k-1$; u_{1d}^{k-1} and u_{1q}^{k-1} are the *dq*-axis components of the first voltage vector at the moment of $k-1$; u_{2d}^{k-1} and u_{2q}^{k-1} are the *dq*-axis components of the second voltage vector at the moment of $k-1$; t_1^{k-1} and t_2^{k-1} are the action times of the first and second voltage vectors at the moment of $k-1$, respectively.

Since the SPMSM electrical time constant is much smaller than the mechanical time constant, the rotational speed can be assumed to be constant during the adjacent control cycle. Then the predicted current at moment k for parameter mismatch

$$\begin{cases} i_{dm}^k = \left(1 - \frac{T_s \tilde{R}_s}{\tilde{L}_s}\right) i_d^{k-1} + T_s \omega_e i_q^{k-1} + \frac{1}{\tilde{L}_s} T_s u_{sd}^{k-1} \\ i_{qm}^k = \left(1 - \frac{T_s \tilde{R}_s}{\tilde{L}_s}\right) i_q^{k-1} - T_s \omega_e i_d^{k-1} + \frac{1}{\tilde{L}_s} T_s u_{sq}^{k-1} \\ \qquad - \frac{T_s \omega_e \tilde{\psi}_f}{\tilde{L}_s} \end{cases} \tag{30}$$

where i_{dpm}^k and i_{qpm}^k are the *dq*-axis predicted current at moment k of parameter mismatch.

Eq. (28) is subtracted from Eq. (30) to obtain the prediction error of the *dq*-axis current at moment $k(E_d^k, E_q^k)$, expressed as follows:

$$\begin{cases} E_d^k = \frac{L_s \Delta R - R_s \Delta L}{L_s (L_s + \Delta L_s)} T_s i_d^{k-1} + \frac{\Delta L}{L_s (L_s + \Delta L)} T_s u_{sd}^{k-1} \\ E_q^k = \frac{L_s \Delta R - R_s \Delta L}{L_s (L_s + \Delta L)} T_s i_q^{k-1} + \frac{\Delta L_s}{L_s (L_s + \Delta L)} T_s u_{sq}^{k-1} \\ \qquad + \frac{L_s \Delta\psi_f - \Delta L \psi_f}{L_s (L_s + \Delta L)} T_s \omega_e \end{cases} \tag{31}$$

Because of the very short control period, the variation of the motor parameters in the adjacent cycles is very small. The prediction error of the *dq*-axis current at the moment $k-1(E_d^{k-1}, E_q^{k-1})$ expressed as follows:

$$\begin{cases} E_d^{k-1} = \frac{L_s \Delta R - R_s \Delta L}{L_s (L_s + \Delta L)} T_s i_d^{k-2} + \frac{\Delta L}{L_s (L_s + \Delta L)} T_s u_{sd}^{k-2} \\ E_q^{k-1} = \frac{L_s \Delta R - R_s \Delta L_s}{L_s (L_s + \Delta L)} T_s i_q^{k-2} \\ \qquad + \frac{\Delta L}{L_s (L_s + \Delta L)} T_s u_{sq}^{k-2} + \frac{L_s \Delta\psi_f - \Delta L \psi_f}{L_s (L_s + \Delta L)} T_s \omega_e \end{cases} \tag{32}$$

$$\begin{cases} T_s u_{sd}^{k-2} = t_1^{k-2} u_{1d}^{k-2} + t_2^{k-2} u_{2d}^{k-2} \\ T_s u_{sq}^{k-2} = t_1^{k-2} u_{1q}^{k-2} + t_2^{k-2} u_{2q}^{k-2} \end{cases} \tag{33}$$

in the above equation, u_{1d}^{k-2} and u_{1q}^{k-2} are the *dq*-axis components of the first voltage vector at the moment of $k-2$; u_{2d}^{k-2} and u_{2q}^{k-2} are the *dq*-axis components of the second voltage vector at the moment of $k-2$; t_1^{k-1} and t_2^{k-1} are the action times of the first and second voltage vectors, respectively.

Thereby, one can define the difference between the prediction errors of two neighbouring control cycles

$$\Delta E = E(k) - E(k-1) \tag{34}$$

It can be deduced that

$$\begin{cases} \Delta E_d = \frac{L_s \Delta R - R_s \Delta L}{L_s (L_s + \Delta L)} \left(i_d^{k-1} - i_d^{k-2}\right) \\ \qquad + \frac{\Delta L}{L_s (L_s + \Delta L)} T_s (u_{sd}^{k-1} - u_{sd}^{k-2}) \\ \Delta E_q = \frac{L_s \Delta R - R_s \Delta L_s}{L_s (L_s + \Delta L)} \left(i_q^{k-1} - i_q^{k-2}\right) \\ \qquad + \frac{\Delta L}{L_s (L_s + \Delta L)} T_s (u_{sd}^{k-1} - u_{sd}^{k-2}) \end{cases} \tag{35}$$

The steady-state fluctuations in adjacent cycle currents are small, and the *dq*-axis currents are much smaller in amplitude magnitude than the *dq*-axis voltages, which have negligible error variations. Rewrite the above equation as:

$$\begin{cases} \Delta E_d = \frac{\Delta L}{L_s(L_s+\Delta L)} \\ (t_1^{k-1}u_{1d}^{k-1} + t_2^{k-1}u_{2d}^{k-1} - t_1^{k-2}u_{1d}^{k-2} - t_2^{k-2}u_{2d}^{k-2}) \\ \Delta E_q = \frac{\Delta L}{L_s(L_s+\Delta L)} \\ (t_1^{k-1}u_{1q}^{k-1} + t_2^{k-1}u_{2q}^{k-1} - t_1^{k-2}u_{1q}^{k-2} - t_2^{k-2}u_{2q}^{k-2}) \end{cases} \tag{36}$$

From Eq. (36), the uncertainty component ΔL_s can be estimated for several adjacent cycles using the d-axis error, because the estimation error q-axis is relatively larger because the q-axis ignores the variations of parameters, such as rotational speed, than the d-axis. ΔL_s can be expressed as:

$$\Delta L \approx \frac{\Delta E_d L^2}{\left(t_1^{k-1}u_{1d}^{k-1} + t_2^{k-1}u_{2d}^{k-1} - t_1^{k-2}u_{1d}^{k-2} - t_2^{k-2}u_{2d}^{k-2}\right)} \tag{37}$$

The estimated inductor can be obtained

$$\tilde{L}_s = L_s + \Delta L_s = L_s + \frac{\Delta E_d L_s^2}{\left(t_1^{k-1}u_{1d}^{k-1} + t_2^{k-1}u_{2d}^{k-1} - t_1^{k-2}u_{1d}^{k-2} - t_2^{k-2}u_{2d}^{k-2}\right)} \tag{38}$$

Due to the short sampling cycle, the degree of inductor variation during the short cycle should be very small. So, after filtering the L_s, the value of the actual inductance can be estimated, and the estimated new inductor value can be added to the model for predictive control.

4.2.2. ESO Observer Current Prediction Error Compensation

By estimating the inductance, a more accurate stator inductance can be obtained; therefore, more accurate predictions can be achieved. Due to the inclusion of differential processes in the mathematical model of the motor, which results in the updated motor parameters, all contain a little fluctuation.

In order to eliminate the disturbances caused by fluctuations in other parameters, the current is observed with an ESO observer. By considering other parameter disturbances and other unknown disturbances as overall disturbances, they can be eliminated. In this paper, two first-order linear ESO observers are used for *dq*-axis current estimation, respectively.

The Eulerian discretization of the *dq*-axis current taking into account parametric disturbances is as follows:

$$\begin{bmatrix} i_d^{k+1} \\ i_q^{k+1} \end{bmatrix} = \left(T_s\widehat{\mathbf{A}} + \mathbf{I}\right)\begin{bmatrix} i_d^k \\ i_q^k \end{bmatrix} + T_s\widehat{\mathbf{C}} + T_s\widehat{\mathbf{B}}\begin{bmatrix} u_d^k \\ u_q^k \end{bmatrix} + T_s\begin{bmatrix} D_d^k \\ D_q^k \end{bmatrix} \tag{39}$$

where $\mathbf{I}$ is the unit matrix, and $\widehat{\mathbf{A}} = \begin{bmatrix} -\tilde{R}_s/\tilde{L}_s & \omega_e \\ -\omega_e & -\tilde{R}_s/\tilde{L}_s \end{bmatrix}$, $\widehat{\mathbf{B}} = \begin{bmatrix} 1/\tilde{L}_s & 0 \\ 0 & 1/\tilde{L}_s \end{bmatrix}$, $\widehat{\mathbf{C}} = \begin{bmatrix} 0 \\ -\omega_e\tilde{\psi}_f/\tilde{L}_s \end{bmatrix}$. D_d^k and D_q^k are the total *dq*-axis disturbances at the moment k, which mainly include the disturbances caused by the changes of motor parameters and reference currents.

From Eq. (39), in order to accurately predict the current, it is necessary to obtain the total *dq*-axis perturbation at the moment k. Design ESO for *dq*-axis currents separately to observe disturbances on real time basis

$$\begin{cases} e_d = \hat{i}_d - i_d \\ p\hat{i}_d = u_d/\hat{L}_s + f_d + \hat{D}_d - \beta_{d1}e_d \\ p\hat{D}_d = -\beta_{d2}e_d \\ f_d = \omega_e i_q - \tilde{R}_s i_d/\tilde{L}_s \end{cases} \tag{40}$$

$$\begin{cases} e_q = \hat{i}_q - i_q \\ p\hat{i}_q = u_q/\hat{L}_s + f_q + \hat{D}_q - \beta_{q1}e_q \\ p\hat{D}_q = -\beta_{q2}e_q \\ f_q = -\tilde{R}_s i_q/\tilde{L}_s - \omega_e i_d - \omega_e\tilde{\psi}_f/\tilde{L}_s \end{cases} \tag{41}$$

in Eqs. (39)∼(41), $\hat{i}_d$, $\hat{i}_q$ are the estimated *dq*-axis currents; $\hat{D}_q$, $\hat{D}_d$ are the observed values of the *dq*-axis, respectively; β_{d1}, β_{d2} and β_{q1}, β_{q2} are the *dq*-axis observer gains, which can be set as:

$$\begin{cases} \beta_{d1} = \beta_{q1} = 2\omega_o \\ \beta_{d2} = \beta_{q2} = \omega_o^2 \end{cases} \tag{42}$$

where ω_o is the observer bandwidth.

Based on the disturbance observation, the predicted current equation is as:

$$\begin{bmatrix} i_d^{k+1} \\ i_q^{k+1} \end{bmatrix} = \left(T_s\widehat{\mathbf{A}} + \mathbf{I}\right)\begin{bmatrix} \hat{i}_d^k \\ \hat{i}_q^k \end{bmatrix} + T_s\widehat{\mathbf{C}} + T_s\widehat{\mathbf{B}}\begin{bmatrix} u_d^k \\ u_q^k \end{bmatrix} + T_s\begin{bmatrix} \hat{D}_d^k \\ \hat{D}_q^k \end{bmatrix} \tag{43}$$

where $\hat{i}_d^k$ and $\hat{i}_q^k$ are the estimates of the observer's *dq*-axis at moment k, respectively.

To sum up, the overall control block diagram of the proposed ERD-MPTC strategy in this paper is shown in Fig. 4.

TABLE 2. SPMSM parameters.

Parameter	Value
Rated speed n_N/(r/min)	1500
DC voltage V_{dc}/(V)	311
Stator inductance L_s/mH	0.00484
Stator resistance R_s/Ω	1.344
Permanent magnet flux ψ_f/Wb	0.267
Number of poles P_n	4
Moment of inertia J/(kg·m^2)	0.01

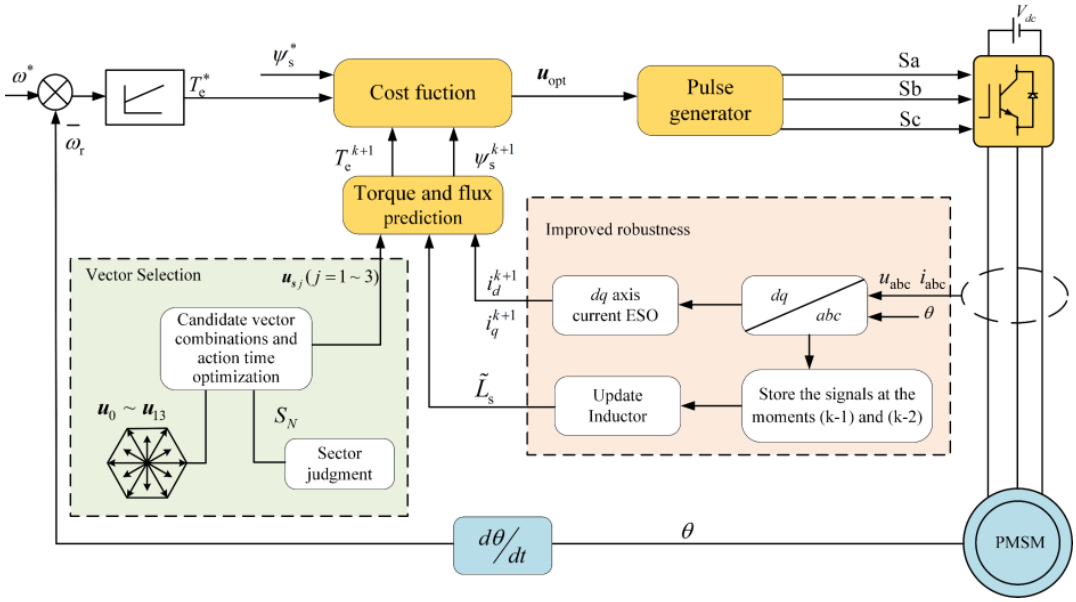

FIGURE 4. Proposed overall control block diagram of the ERD-MPTC strategy.

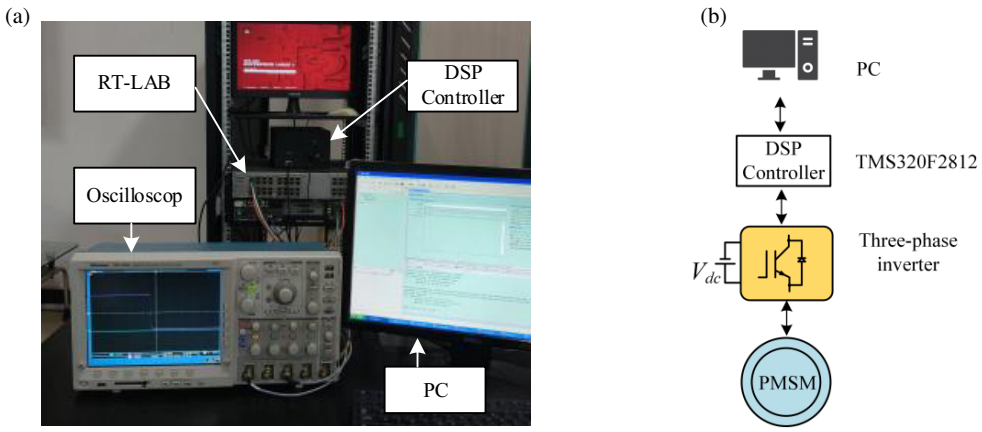

FIGURE 5. RT-LAB experiment platform and hardware in the loop system configuration. (a) RT-LAB experiment platform. (b) Hardware in the loop system configuration.

5. EXPERIMENTAL VERIFICATION

In order to verify the proposed ID-MPTC strategy's torque pulsation suppression effect and the IRD-MPTC strategy's robustness enhancement effect during parameter mismatch, the three-phase SPMSM is experimentally verified, and the obtained experimental data are analyzed. The experiment equipment is RT-LAB semi-physical experiment platform, as shown in Fig. 5(a). The controller takes TMS320F2812 as the core; the PMSM system, inverter, etc. are constructed using RT-LAB (op5600); and its hardware system configuration is shown in Fig. 5(b). The SPMSM parameters are shown in Table 2. To fairly reflect the effect of the control strategy proposed in this paper, the same PI parameters of the speed outer loop are used during the experiments.

5.1. Experimental Verification of ID-MPTC Performance

In order to verify the improvement in the steady state performance of the ID-MPTC proposed in this paper, a comparison is made with the Literature [10] proposal of the ID-MPTC control strategy. The motor starts with a load of 5 N·m and given speed of 1000 r/min.

The experimental results are shown in Fig. 6, where the torque, magnetic chain, and A-phase current are represented from top to bottom. From the torque waveform graph in Fig. 6, it can be seen that the output torque of the proposed ID-MPTC is smoother and has less torque pulsation than the ID-MPTC. From Fig. 6, it can be seen that the maximum torque ripple of the ID-MPTC proposed in this paper and the ID-MPTC proposed in [10] are 0.79 N·m, 1.23 N·m, respectively. It can be seen that the maximum torque ripple of the proposed ID-MPTC is 0.44 N·m lower than that of the ID-MPTC proposed in [10], and the ratio η of the maximum torque ripple to the load torque is reduced by about 9%, which reduces the torque output pulsation, and thus improves the steady state torque performance of the motor. The A-phase current total harmonic distortion rate (THD) of ID-MPTC proposed in this paper and ID-MPTC proposed in [10] are 8.44% and 5.71%, respectively. In contrast,

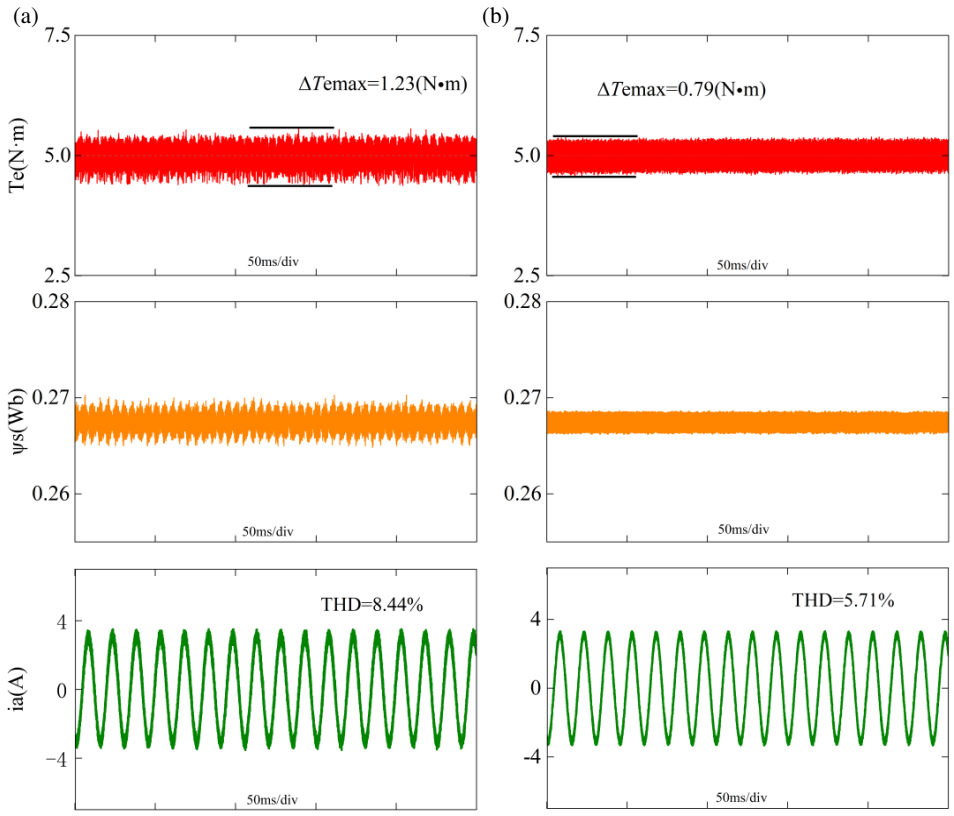

FIGURE 6. Steady state performance comparison of two control strategies. (a) The proposed ID-MPTC in literature [10]. (b) The proposed ID-MPTC in this paper.

TABLE 3. Comparison of the performance data of the two control strategies at steady state.

Parameter	ID-MPTC [10]	Proposed ID-MPTC
Te_H/(N·m)	5.59	5.39
Te_L/(N·m)	4.36	4.60
$\Delta T_{e\,\max}$/(N·m)	1.23	0.79
η	24.6%	15.8%
THD	8.44%	5.71%

(Te_H and Te_L are the upper and lower boundaries of steady state torque ripple;
$\Delta T_{e\,\max}$ is the maximum torque ripple;
η is the ratio of maximum torque ripple to load torque 5 N·m)

the proposed ID-MPTC strategy in this paper can reduce the phase current THD by about 2.7%. This is the main reason that makes the torque output ripple to be reduced. Since some flux ripple cases are considered in terms of cost function while using deadbeat torque control, it can be seen from Fig. 6 that the improved stator flux ripple is significantly smaller than the ID-MPTC proposed in [10]. The above experimental results show that the improved dual-vector control strategy can effectively improve the operating performance of the motor in steady state. Specific experimental data comparisons are shown in Table 3.

To further verify the performance of the ID-MPTC strategy in terms of dynamic response, the motor is made to start with a load of 2 N·m, and when it is stabilized; at 0.2 s, the load torque suddenly increases to 4 N·m; at 0.3 s, the given rotational speed jumps from 1000 r/min to 1200 r/min.

The experimental results are shown in Fig. 7, where torque, speed, and A-phase current are represented from top to bottom. Since the MPTC control strategy inherits the fast torque dynamic response performance of direct torque control (DTC), the proposed ID-MPTC and [10] proposed ID-MPTC also have fast dynamic response. It can also be seen from Fig. 7 that in terms of torque dynamic response performance, the ID-MPTC proposed in this paper is basically the same as the ID-MPTC proposed in [10]. The output torque responds quickly to sudden changes in load torque and speed. When the load changes suddenly, the speed of both control strategies also has a good tracking effect, basically no overshoot. The phase currents are also

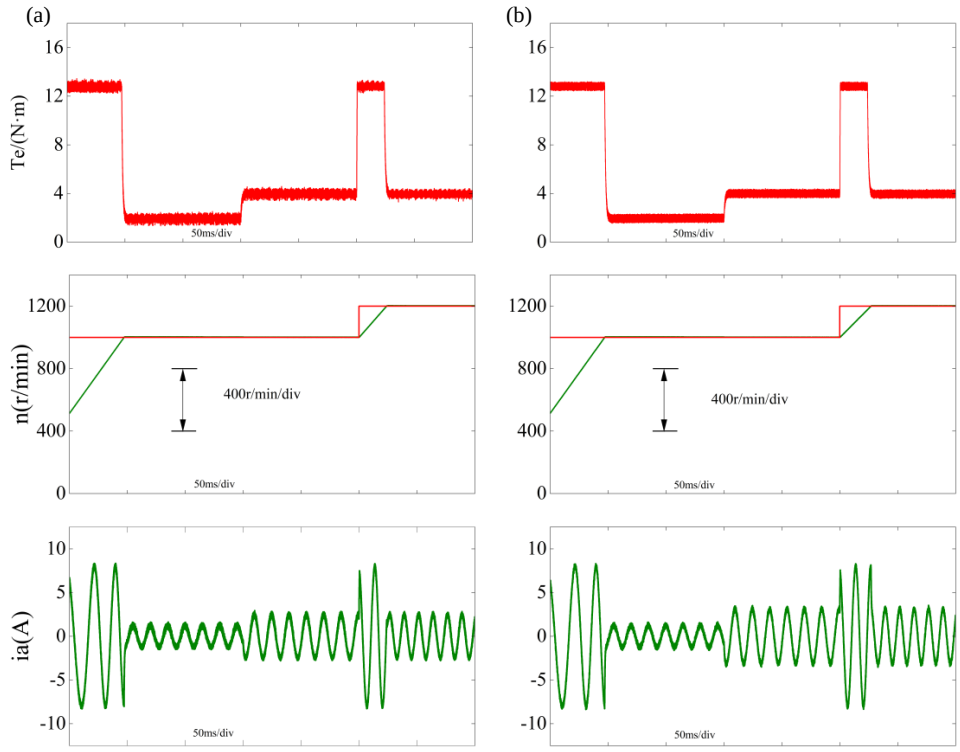

FIGURE 7. Dynamic performance comparison of two control strategies. (a) Literature [10] proposed the ID-MPTC. (b) The proposed ID-MPTC in this paper.

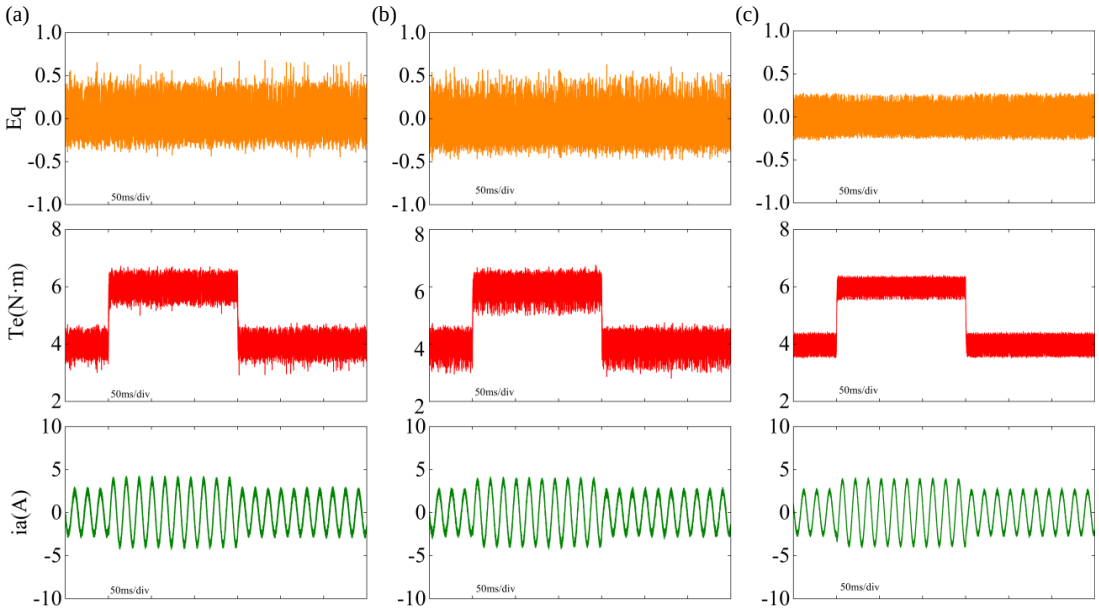

FIGURE 8. Comparison of motor performance for three control strategies with parameter mismatch ($\tilde{L}_s = 3L_s$, $\tilde{\psi}_f = 2\psi f$, $\tilde{R}_s = 0.5R_s$). (a) ID-MPTC [10]. (b) Proposed ID-MPTC. (c) Proposed IRD-MPTC.

smoother for both control strategies. It is shown through experiments that the proposed improved control strategy enhances the steady state performance along with a faster dynamic response.

5.2. IRD-MPTC Strategy Experimental Validation

The experimental working conditions are as follows: the motor is started with a load of 4 N·m, and when it is stabilized, at 0.2 s the load torque suddenly increases to 6 N·m; at 0.35 s, the load torque decreases to 4 N·m.

Figure 8 shows the performance comparison of the three control strategies, proposed ID-MPTC in [10], proposed ID-MPTC and ERD-MPTC in this paper, under parameter mismatch ($\tilde{L}_s = 3L_s$, $\tilde{\psi}_f = 2\psi f$, $\tilde{R}_s = 0.5R_s$). In Fig. 8, from top to bottom are the q-axis current error, torque, and A-phase

TABLE 4. Comparison of experimental data of torque mutation of three control strategies.

Parameter	ID-MPTC [10]	Proposed ID-MPTC	Proposed IRD-MPTC
Te_H/(N·m)	6.71	6.78	6.40
Te_L/(N·m)	5.01	5.03	5.54
$\Delta T_{e\,\max}$/(N·m)	1.70	1.75	0.86
η	28.3%	29.2%	14.3%
Eq (A)	0.54	0.57	0.27

(η is the ratio of maximum torque ripple to load torque 6 N·m; Eq is the q-axis current error)

current. From Fig. 8, it can be seen that both proposed ID-MPTC and [10] proposed ID-MPTC show poor system performance under parameter mismatched operating conditions. But the ERD-MPTC still delivers excellent performance. Specific experimental data comparisons are shown in Table 4.

The q-axis current error represents the difference between the predicted value and the given current value, which is a good indicator of how well the predicted current is tracking. It can be seen from Fig. 8 that the ERD-MPTC strategy has a smoother q-axis current error curve than the other two control strategies. At parameter mismatch, the q-axis current errors of the three control strategies, ID-MPTC [10], ID-MPTC, and ERD-MPTC, are 0.54 A, 0.57 A, and 0.27 A, respectively. The ERD-MPTC strategy reduces the q-axis current error by 0.27 A, 0.3 A, respectively. When the parameters are changed, the inductance updating mechanism and the introduction of the observer can effectively solve the problem of the large error of the predicted current.

In the case of parameter mismatch, from the torque plots in Fig. 8, it can be seen that the output torque of the ID-MPTC [10] and the proposed ID-MPTC strategy undergoes severe oscillations, which can seriously deteriorate the performance of the motor. However, the ERD-MPTC strategy torque is still smoothly output with low pulsations. The maximum torque pulsations of ID-MPTC [10], the proposed ID-MPTC, and ERD-MPTC control strategies are 1.70 N·m, 1.75 N·m, and 0.86 N·m, respectively. The ratio of maximum torque ripple to load torque η is 28.3%, 29.2%, and 14.3%, respectively. The ERD-MPTC strategy compared with the ID-MPTC proposed in [10] and the ID-MPTC proposed in this paper reduces the maximum torque pulsation by about 0.84 N·m and 0.9 N·m, respectively. The ratio of maximum torque pulsation to load torque η is reduced by 14% and 15%, respectively.

It can also be seen from Fig. 8 that the torque dynamic response speeds of the three control methods are basically the same. In contrast, the A-phase current burr of the ERD-MPTC strategy is smaller. Experiments show that the ERD-MPTC control strategy has the same fast dynamic response performance as MPTC. The experimental data and waveforms show that, in the face of motor parameter variations, the proposed IRD-MPTC strategy makes the motor operation still perform well and improves the parameter robustness of the system.

6. CONCLUSION

Aiming at the problems of traditional dual-vector control with large computation, large torque pulsation, and control performance that is seriously dependent on the accuracy of motor parameters. This paper proposes an enhanced robustness dual-vector model predictive control strategy for permanent magnet synchronous motors, and verifies the effectiveness of its strategy. The following conclusions can be drawn:

(1) Compared with the voltage vector selection of the traditional dual-vector MPTC, the proposed ID-MPTC reduces the number of iterations from 14 to 3. The weight coefficients are eliminated in the cost function at the same time, and the fluctuation of the switching point moment is also considered in the cost function, which reduces the complexity of the algorithm.

(2) Compared with the traditional ID-MPTC, the proposed ID-MPTC strategy reduces the steady-state maximum torque ripple by 0.44 N·m and reduces the phase current THD by about 2.7%, which effectively improves the performance of the system during steady-state operation.

(3) Due to the inclusion of inductor updating mechanism and ESO disturbance observation to the proposed ID-MPTC, the proposed ERD-MPTC strategy reduces the detrimental effect on ID-MPTC in the case of parameter mismatch and improves the parameter robustness of the system.

ACKNOWLEDGEMENT

This work was supported by the Natural Science Foundation of Hunan Province of China under Grant Number 2023JJ50191, Educational Commission of Hunan Province of China under Grant Number 21B0552.

REFERENCES

[1] Xu, S., *et al.*, "A minor fault diagnosis for current sensor of new energy vehicle drive system based on adaptive sliding mode observer," *Proceedings of the CSEE*, Vol. 43, No. 18, 7277, 2023.

[2] Song, J.-L., D.-K. Qu, F. Xu, and F.-S. Zou, "Active compliance control research for robots without force sensor," *Electric Machines and Control*, Vol. 24, No. 8, 160, 2020.

[3] Rodriguez, J., M. P. Kazmierkowski, J. R. Espinoza, P. Zanchetta, H. Abu-Rub, H. A. Young, and C. A. Rojas, "State of the art of finite control set model predictive control in power electronics," *IEEE Transactions on Industrial Informatics*, Vol. 9, No. 2, 1003–1016, May 2013.

[4] Rodriguez, J., C. Garcia, A. Mora, F. Flores-Bahamonde, P. Acuna, M. Novak, Y. Zhang, L. Tarisciotti, S. A. Davari, Z. Zhang, F. Wang, M. Norambuena, T. Dragicevic, F. Blaabjerg, T. Geyer, R. Kennel, *et al.*, "Latest advances of model predictive control in electrical drives - Part I: Basic concepts and advanced strategies," *IEEE Transactions on Power Electronics*, Vol. 37, No. 4, 3927–3942, 2022.

[5] Rodriguez, J., C. Garcia, A. Mora, S. A. Davari, J. Rodas, D. F. Valencia, M. Elmorshedy, F. Wang, K. Zuo, L. Tarisciotti, F. Flores-Bahamonde, W. Xu, Z. Zhang, Y. Zhang, M. Norambuena, A. Emadi, T. Geyer, R. Kennel, T. Dragicevic, D. A. Khaburi, Z. Zhang, M. Abdelrahem, and N. Mijatovic, "Latest advances of model predictive control in electrical drives - Part II: Applications and benchmarking with classical control methods," *IEEE Transactions on Power Electronics*, Vol. 37, No. 5, 5047–5061, May 2022.

[6] Wu, M., X. Sun, J. Zhu, G. Lei, and Y. Guo, "Improved model predictive torque control for PMSM drives based on duty cycle optimization," *IEEE Transactions on Magnetics*, Vol. 57, No. 2, 1–5, Feb. 2021.

[7] Yu, H., J. Deng, and Y. Li, "A diagnosis method of semiconductor power switch open-circuit fault in the PMSM drive system with the MPCC method," *IEEE Access*, Vol. 9, 109 822–109 832, 2021.

[8] Davari, S. A., D. A. Khaburi, and R. Kennel, "An improved FCS-MPC algorithm for an induction motor with an imposed optimized weighting factor," *IEEE Transactions on Power Electronics*, Vol. 27, No. 3, 1540–1551, Mar. 2012.

[9] Xu, Y., B. Zhang, and Q. Zhou, "Two-vector based model predictive current control for permanent magnet synchronous motor," *Transactions of China Electrotechnical Society*, Vol. 32, No. 20, 222–230, 2017.

[10] Wu, M., X. Sun, J. Zhu, G. Lei, and Y. Guo, "Improved model predictive torque control for PMSM drives based on duty cycle optimization," *IEEE Transactions on Magnetics*, Vol. 57, No. 2, 1–5, Feb. 2021.

[11] Lan, Z., B. Wang, C. Xu, and L. Li, "A novel three-vector model predictive current control for permanent magnet synchronous motor," *Proceedings of the CSEE*, Vol. 38, 243–249, 2018.

[12] Wang, Z., X. Zhang, and Y. Guo, "Three-vector predictive current control for interior permanent magnet synchronous motor," in *6th IEEE International Conference on Predictive Control of Electrical Drives and Power Electronics (PRECEDE 2021)*, 443–448, Jinan, China, Nov. 2021.

[13] Xiao, Q., Z. Li, B. Luo, T. Wang, D. Wen, and Y. Zhang, "Improved three vector model predictive torque control of PMSM," *Progress In Electromagnetics Research M*, Vol. 109, 217–229, 2022.

[14] Shi, T., Y. Yang, Z. Zhou, Q. Geng, and C. Xia, "FCS-MPC for dual-motor torque synchronization system based on quadratic form cost function," *Proceedings of the CSEE*, Vol. 39, No. 15, 4531–4541, 2019.

[15] Rojas, C. A., J. R. Rodriguez, S. Kouro, and F. Villarroel, "Multiobjective fuzzy-decision-making predictive torque control for an induction motor drive," *IEEE Transactions on Power Electronics*, Vol. 32, No. 8, 6245–6260, Aug. 2017.

[16] Novak, M., H. Xie, T. Dragicevic, F. Wang, J. Rodriguez, and F. Blaabjerg, "Optimal cost function parameter design in predictive torque control (PTC) using artificial neural networks (ANN)," *IEEE Transactions on Industrial Electronics*, Vol. 68, No. 8, 7309–7319, Aug. 2021.

[17] Kim, S., J. Park, J. Bae, K. Cho, and D.-H. Lee, "An advanced multiple predictive direct torque control of PMSM using PWM and the 12 sectors," in *2019 IEEE 6th International Conference on Industrial Engineering and Applications (ICIEA)*, 27–32, Tokyo, Apr. 2019.

[18] Zhang, Y., W. Xie, Z. Li, and Y. Zhang, "Low-complexity model predictive power control: Double-vector-based approach," *IEEE Transactions on Industrial Electronics*, Vol. 61, No. 11, 5871–5880, Nov. 2014.

[19] Sawma, J., F. Khatounian, E. Monmasson, L. Idkhajine, and R. Ghosn, "Analysis of the impact of online identification on model predictive current control applied to permanent magnet synchronous motors," *IET Electric Power Applications*, Vol. 11, No. 5, 864–873, 2017.

[20] Yan, L., F. Wang, M. Dou, Z. Zhang, R. Kennel, and J. Rodriguez, "Active disturbance-rejection-based speed control in model predictive control for induction machines," *IEEE Transactions on Industrial Electronics*, Vol. 67, No. 4, 2574–2584, Apr. 2020.

[21] Li, X., W. Tian, X. Gao, Q. Yang, and R. Kennel, "A generalized observer-based robust predictive current control strategy for PMSM drive system," *IEEE Transactions on Industrial Electronics*, Vol. 69, No. 2, 1322–1332, 2021.

[22] Zhang, X., L. Zhang, and Y. Zhang, "Model predictive current control for PMSM drives with parameter robustness improvement," *IEEE Transactions on Power Electronics*, Vol. 34, No. 2, 1645–1657, Feb. 2019.

[23] Yuan, X., S. Zhang, and C. Zhang, "Improved model predictive current control for SPMSM drives with parameter mismatch," *IEEE Transactions on Industrial Electronics*, Vol. 67, No. 2, 852–862, Feb. 2020.

[24] Yuan, X., S. Zhang, and C. Zhang, "Nonparametric predictive current control for PMSM," *IEEE Transactions on Power Electronics*, Vol. 35, No. 9, 9332–9341, Sep. 2020.

[25] Wang, F., K. Zuo, P. Tao, and J. Rodriguez, "High performance model predictive control for PMSM by using stator current mathematical model self-regulation technique," *IEEE Transactions on Power Electronics*, Vol. 35, No. 12, 13 652–13 662, Dec. 2020.

[26] Yuan, X., Y. Zuo, Y. Fan, and C. H. T. Lee, "Model-free predictive current control of SPMSM drives using extended state observer," *IEEE Transactions on Industrial Electronics*, Vol. 69, No. 7, 6540–6550, Jul. 2022.

[27] Lin, C.-K., J.-T. Yu, Y.-S. Lai, and H.-C. Yu, "Improved model-free predictive current control for synchronous reluctance motor drives," *IEEE Transactions on Industrial Electronics*, Vol. 63, No. 6, 3942–3953, Jun. 2016.

[28] Kim, H., J. Han, Y.-I. Lee, J.-H. Song, and K.-B. Lee, "Torque predictive control of permanent-magnet synchronous motor using duty ratio prediction," in *2013 IEEE International Symposium on Industrial Electronics (ISIE)*, 1–5, Taipei, Taiwan, May 2013.